FERMILAB-PUB-07-058-E

Precision measurements of the total and partial widths of the $\psi(2S)$ charmonium meson with a new complementary-scan technique in $\bar{p}p$ annihilations

Fermilab E835 Collaboration

M. Andreotti, [b] S. Bagnasco, [c,g] W. Baldini, [b] D. Bettoni, [b] G. Borreani, [g] A. Buzzo, [c] R. Calabrese, [b] R. Cester, [g] G. Cibinetto, [b] P. Dalpiaz, [b] G. Garzoglio, [a] K. E. Gollwitzer, [a] M. Graham, [e] M. Hu, [a] D. Joffe, [f] J. Kasper, [f] G. Lasio, [d] M. Lo Vetere, [c] E. Luppi, [b] M. Macrì, [c] M. Mandelkern, [d] F. Marchetto, [g] M. Marinelli, [c] E. Menichetti, [g] Z. Metreveli, [f] R. Mussa, [b,g] M. Negrini, [b] M. M. Obertino, [e,g] M. Pallavicini, [c] N. Pastrone, [g] C. Patrignani, [c] S. Pordes, [a] E. Robutti, [c] W. Roethel, [d,f] J. Rosen, [f] P. Rumerio, [f] R. W. Rusack, [e] A. Santroni, [c] J. Schultz, [d] S. H. Seo, [e] K. K. Seth, [f] G. Stancari, [a,b,*] M. Stancari, [b,d] A. Tomaradze, [f] I. Uman, [f] T. Vidnovic, [e] S. Werkema, [a] P. Zweber [f]

[a] *Fermi National Accelerator Laboratory, Batavia, IL 60510, USA*

[b] *Istituto Nazionale di Fisica Nucleare and University of Ferrara, 44100 Ferrara, Italy*

[c] *Istituto Nazionale di Fisica Nucleare and University of Genova, 16146 Genova, Italy*

[d] *University of California, Irvine, CA 92697, USA*

[e] *University of Minnesota, Minneapolis, MN 55455, USA*

Preprint submitted to Elsevier Science *28 February 2007*

[f]*Northwestern University, Evanston, IL 60208, USA*

[g]*Istituto Nazionale di Fisica Nucleare and University of Torino, 10125 Torino, Italy*

Abstract

We present new precision measurements of the $\psi(2S)$ total and partial widths from excitation curves obtained in antiproton-proton annihilations by Fermilab experiment E835 at the Antiproton Accumulator in the year 2000. A new technique of complementary scans was developed to study narrow resonances with stochastically cooled antiproton beams. It relies on precise revolution-frequency and orbit-length measurements, while making the analysis of the excitation curve almost independent of machine lattice parameters. For the $\psi(2S)$ meson, by studying the processes $\bar{p}p \to e^+e^-$ and $\bar{p}p \to J/\psi + X \to e^+e^- + X$, we measure the width $\Gamma = 290 \pm 25(\text{sta}) \pm 4(\text{sys})$ keV and the combination of partial widths $\Gamma_{e^+e^-}\Gamma_{\bar{p}p}/\Gamma = 579 \pm 38(\text{sta}) \pm 36(\text{sys})$ meV, which represent the most precise measurements to date.

Key words:

PACS: 14.40.Gx, 13.20.Gd, 13.75.Cs, 29.27.Fh

1 Introduction

A precise measurement of the excitation curve of narrow charmonium resonances depends both on the detection technique (event statistics, detector efficiency) and on the properties of the beam-energy spectrum. In e^+e^- annihilations, one can collect high statistics to compensate for the beam energy spread being substantially larger

* Corresponding author: Dr. Giulio Stancari, Istituto Nazionale di Fisica Nucleare, Via Saragat 1, I-44100 Ferrara FE, Italy. Phone: +39.0532.974330; fax: +39.0532.974343; e-mail: `stancari@fe.infn.it`.

than the resonance width. The BES Collaboration at BEPC recently published two measurements of the $\psi(2S)$ width based on its large samples [1,2]. The combination $\Gamma_{e^+e^-}\Gamma_{\bar{p}p}/\Gamma$ was recently measured by the BABAR Collaboration [3]. In $\bar{p}p$ annihilations, the event statistics are lower, but one can take advantage of stochastically cooled antiproton beams, with FWHM energy spreads of 0.4–0.5 MeV in the center-of-mass frame. Fermilab experiment E760 measured the widths of the J/ψ and $\psi(2S)$ mesons [4]. The uncertainty was dominated by event statistics and statistical fluctuations in the beam position measurements. A sizeable systematic uncertainty was due to the measurement of the beam-energy spectrum. In this paper, we present results obtained in $\bar{p}p$ annihilations by Fermilab experiment E835 from data collected during the year 2000 run. A new scanning technique, together with higher event statistics, improvements in the beam position measurement and momentum-spread analysis, allow us to reach the highest precision to date.

2 Experiment technique

In experiment E835, antiprotons circulating in the Antiproton Accumulator intersect an internal hydrogen gas jet target. The beam is cooled and decelerated to scan charmonium resonances. The operation of the Accumulator for E835 is described in Ref. [5].

The E835 detector is a nonmagnetic spectrometer designed to extract, from the hadronic background, clean electron-positron pairs of high invariant mass as a signature of charmonium formation. Ref. [6] describes the experiment in detail.

The resonance parameters are determined from a maximum-likelihood fit to the excitation curve. For each data-taking run (subscript i), we assume that the average number of observed events μ_i in each channel is the product of a Breit-Wigner cross section $\sigma_{\rm BWr}$ with constant background $\sigma_{\rm bkg}$ and the center-of-mass energy distribution, B_i:

$$\mu_i = \mathscr{L}_i \left[\varepsilon_i \int \sigma_{\rm BWr}(w) B_i(w)\, dw + \sigma_{\rm bkg} \right], \tag{1}$$

where w is the center-of-mass energy, ε_i is the detector efficiency, $\mathscr{L}_i$ is the integrated luminosity, and the integral is extended over the energy acceptance of the machine. The spin-averaged Breit-Wigner cross section for a spin-J resonance of mass M and width Γ formed in $\bar{p}p$ annihilations is

$$\sigma_{\rm BW}(w) = \frac{(2J+1)}{(2S+1)^2} \frac{16\pi}{w^2 - 4m^2} \frac{(\Gamma_{\rm in}\Gamma_{\rm out}/\Gamma)\cdot\Gamma}{\Gamma^2 + 4(w-M)^2}; \tag{2}$$

m and S are the (anti)proton mass and spin, while $\Gamma_{\rm in}$ and $\Gamma_{\rm out}$ are the partial resonance widths for the entrance ($\bar{p}p$, in our case) and exit channels. The Breit-Wigner cross section is corrected for initial-state radiation to obtain $\sigma_{\rm BWr}$ [4,7]:

$$\sigma_{\rm BWr}(w) = b \int_0^{w/2} \frac{dk}{k} \left(\frac{2k}{w}\right)^b \sigma_{\rm BW}(\sqrt{w^2 - 2kw}) \tag{3}$$

$$= (2/w)^b \int_0^{(w/2)^b} dt\, \sigma_{\rm BW}(\sqrt{w^2 - 2t^{1/b}w}), \tag{4}$$

where the second form is more suitable for numerical integration and $b(w)$ is the semiclassical collinearity factor [7], equal to 0.00753 at the $\psi(2S)$.

The resonance mass M, width Γ, ‘area’ $(\Gamma_{\rm in}\Gamma_{\rm out}/\Gamma)$ and the background cross section $\sigma_{\rm bkg}$ are left as free parameters in the maximization of the log-likelihood function $\log(\Lambda) = \sum_i \log P(\mu_i, N_i)$, where $P(\mu, N)$ are Poisson probabilities of observing N events when the mean is μ.

Both channels $\bar{p}p \to e^+e^-$ and $\bar{p}p \to J/\psi + X \to e^+e^- + X$ are fit simultaneously to the same mass and width. Each channel is allowed its own area and background cross section, for a total of 6 fit parameters. [1]

Two scans of the $\psi(2S)$ resonance were performed. For each run i, the number of events N_i, luminosity $\mathscr{L}_i$ and efficiency ε_i are shown in Tables 1 and 2. The event selection is described in our paper on $\psi(2S)$ branching ratios [8].

3 Beam energy measurements

The center-of-mass energy distribution $B_i(w)$ is critical for width and area measurements. We summarize here the concepts that are essential for the following discussion. More details can be found in Refs. [4,5].

The beam-frequency distribution is accurately measured by detecting the Schottky noise signal generated by the coasting beam. The signal is sensed by a 79-MHz longitudinal Schottky pickup and recorded on a spectrum analyzer. An accuracy of 0.05 Hz is achieved on a revolution frequency of 0.6 MHz, over a wide dynamic range in intensity (60 dBm).

The beam is slightly bunched, both for stability (ion clearing) and for making the beam position monitors (BPMs) sensitive to a portion of the beam. Therefore, recorded orbits refer to particles revolving at the rf frequency f^{rf} (which is usually close to the average revolution frequency of the beam). Each orbit consists of 48 horizontal and 42 vertical readings. Thanks to new hardware and software, these

[1] The ‘area’ parameter is usually chosen in the parameterization of the resonance shape because it is proportional to the total number of events in each channel. It is less correlated with the width than the product of branching fractions.

readings are much less noisy than E760's [4], as discussed later in the uncertainty estimates.

From the BPM readings and the Accumulator lattice model, we can calculate orbit length differences ΔL very accurately. The main systematic uncertainties come from BPM calibrations, from bend-field drifts, and from neglecting second-order terms in the orbit length. Using the dispersion function from the lattice model, the gains of the high-dispersion BPMs can be measured by varying the beam energy at constant magnetic field. They show scaling errors between 3% and 15%. Their systematic effect on ΔL is about 0.03 mm. Contributions from scaling errors in the low-dispersion BPMs are harder to evaluate, but they should be comparable. Bend-field drifts (due to temperature variations, for instance) appear in the orbit-length calculation as changes in momentum. For the $\psi(2S)$ scans, their contribution translates into an uncertainty in ΔL of about 0.04 mm. The second-order terms depend on the derivatives of the vertical and horizontal orbit slope differences with respect to the reference orbit as well as the slopes of the reference orbit itself. An explicit assessment of these terms is not possible, because there are not enough BPMs to measure slopes everywhere around the ring. Under reasonable assumptions, one would get an error of about 0.005 mm. A test was performed to estimate the accuracy in ΔL. The systematic uncertainty is evaluated by using a January 2000 $\psi(2S)$ orbit to predict the length of a very different $\psi(2S)$ orbit of known length from August 1997, when the machine lattice was also quite different. The difference between the known length and the predicted length is 0.05 mm out of 474 m. Since orbits and lattices for the runs used in this analysis are much closer to each other, this is taken as the systematic uncertainty in ΔL from the beam-energy calculation for these runs.

The length L of an orbit can be calculated from a reference orbit of length L_0:

$L = L_0 + \Delta L$. The absolute calibration of L_0 is done by scanning a charmonium resonance the mass of which is precisely known from the resonant-depolarization method in e^+e^- experiments [9]. For particles in the bunched portion of the beam (rf bucket), the relativistic parameters β^{rf} and γ^{rf} are calculated from their velocity $v^{\mathrm{rf}} = f^{\mathrm{rf}} \cdot L$, from which the center-of-mass energy w of the $\bar{p}p$ system is calculated: $w^{\mathrm{rf}} = w(f^{\mathrm{rf}}, L) \equiv m\sqrt{2\,(1+\gamma^{\mathrm{rf}})}$. (The superscript rf is omitted from orbit lengths because they always refer to particles in the rf bucket.) In the charmonium region, this method yields good accuracies on w. For instance, $\partial w/\partial f = 113$ keV/Hz (38 keV/Hz) and $\partial w/\partial L = 149$ keV/mm (50 keV/mm) at the $\psi(2S)$ (and J/ψ).

For width and area determinations, energy differences are crucial, and they must be determined precisely. In our standard experiments, where we keep the beam near the central orbit of the Accumulator, a particular run is chosen as the reference (subscript 0). Energy differences between the reference run and other runs in the scan (subscript i), for particles in the rf bucket, are simply

$$w_i^{\mathrm{rf}} - w_0^{\mathrm{rf}} = w(f_i^{\mathrm{rf}}, L_0 + \Delta L_i) - w(f_0^{\mathrm{rf}}, L_0). \tag{5}$$

Within the energy range of a resonance scan, these differences are largely independent of the choice of L_0. For this reason, the absolute energy calibration is irrelevant for width and area measurements. Only uncertainties coming from ΔL are considered.

Once the energy w_i^{rf} for particles in the rf bucket is known, the complete energy distribution is obtained from the Schottky spectrum using the relation between frequency differences and momentum differences at constant magnetic field:

$$\frac{\Delta p}{p} = -\frac{1}{\eta}\frac{\Delta f}{f}, \tag{6}$$

where η is the energy-dependent phase-slip factor of the machine, which is one of the parameters governing synchrotron oscillations. (The choice of η as a function of energy is described in Ref. [5]; its variation within a scan can be neglected.) In terms of the center-of-mass energy,

$$w - w_i^{\mathrm{rf}} = -\frac{1}{\eta}\frac{(\beta_i^{\mathrm{rf}})^2(\gamma_i^{\mathrm{rf}})m^2}{w_i^{\mathrm{rf}}}\frac{f - f_i^{\mathrm{rf}}}{f_i^{\mathrm{rf}}}. \tag{7}$$

Within a run, rf frequencies, beam-frequency spectra, and BPM readings are updated every few minutes. Frequency spectra are then translated into center-of-mass energy through Eq. 7, weighted by luminosity and summed, to obtain the luminosity-weighted normalized energy spectra $B_i(w)$ for each data-taking run.

The phase-slip factor is usually determined from the synchrotron frequency. In our case, this determination has a 10% uncertainty coming from the bolometric rf voltage measurement [6]. At the $\psi(2S)$, the synchrotron-frequency method yields a phase-slip factor $\eta = 0.0216 \pm 0.0022$.

The resonance width and area are affected by a systematic error due to the uncertainty in η. Usually, the resonance width and area are positively correlated with the phase-slip factor. A larger η implies a narrower energy spectrum, as described in Eq. 7. As a consequence, the fitted resonance will more closely resemble the measured excitation curve, yielding a larger resonance width. For our scan at the central orbit (stack 1), the 10% uncertainty in η translates into a systematic uncertainty of about 18% in the width and 2% in the area.

4 Complementary scans

For precision measurements, one needs a better estimate of the phase-slip factor or determinations that are independent of η, or both. In E760, this was done with the 'double scan' technique [4], which has the disadvantage of being operationally complex.

Here we describe a new method of 'complementary scans.' The resonance is scanned once on the central orbit, as described above. A second scan is then performed at constant magnetic bend field (most of stack 29, runs 5818–5831). The energy of the beam is changed by moving the longitudinal stochastic-cooling pickups. The beam moves away from the central orbit, and the range of energies is limited but appropriate for narrow resonances.

Since the magnetic field is constant, beam-energy differences can be calculated independently of ΔL, directly from the revolution-frequency spectra and the phase-slip factor, according to Eq. 7. A pivot run is chosen (5827 in our case, subscript p). The rf frequency of this run is used as a reference to calculate the energy for particles in the rf bucket in other runs. These particles have revolution frequency f_i^{rf} and the energy is calculated as follows:

$$w_i^{\mathrm{rf}} - w_p^{\mathrm{rf}} = -\frac{1}{\eta} \frac{(\beta_p^{\mathrm{rf}})^2 (\gamma_p^{\mathrm{rf}}) m^2}{w_p^{\mathrm{rf}}} \frac{f_i^{\mathrm{rf}} - f_p^{\mathrm{rf}}}{f_p^{\mathrm{rf}}}. \qquad (8)$$

For the scan at constant magnetic field, this relation is used instead of Eq. 5. Once the energy for particles at f^{rf} is known, the full energy spectrum within each run is obtained from Eq. 7, as usual. [2]

[2] For the constant-field scan, the energy distributions may be obtained directly from the pivot energy by calculating $w - w_p^{\mathrm{rf}}$, instead of using Eq. 8 first and then Eq. 7. The two-

Using this alternative energy measurement, the width and area determined from scans at constant magnetic field are negatively correlated with η. The increasing width with increasing η is still present, as it is in scans at nearly constant orbit. But the dominant effect is that a larger η brings the energy points in the excitation curve closer to the pivot point, making the width smaller. In the case of stack 29, a 10% increase in η implies a -10% variation in both width and area.

The different dependence of the width on η in the two separate scans is shown as two crossing curves in Figure 1. The constant-orbit and the constant-field scan can be combined. The resulting width has a dependence on η that is intermediate between the two. An appropriate luminosity distribution can make the resulting curve practically horizontal.

Moreover, thanks to this complementary behavior, the width, area and phase-slip factor can be determined in a maximum-likelihood fit where η is also a free parameter. Errors and correlations are then obtained directly from the fit.

5 Results

Both channels in both scans are fitted simultaneously, leaving the phase-slip factor as a free parameter. The energy distributions are rescaled according to Eq. 7 for the 'constant-orbit' scan and Eqs. 7 and 8 for the 'constant-field' scan. The log-likelihood function is $\log(\Lambda) = \sum_i \left[\log P(\mu_i^{ee}, N_i^{ee}) + \log P(\mu_i^{X}, N_i^{X})\right]$. For each

---

step procedure is chosen because it is faster to rescale the energy spectra than to re-calculate them from the frequency spectra when fitting for η. Numerically, the difference between the two calculations is negligible (less than 0.2 keV). Moreover, the two-step procedure exposes how the width depends on η.

channel, the mean numbers of events μ_i^{ee} and μ_i^X are evaluated according to Eq. 1. All runs have the same e^+e^- efficiency $\varepsilon^{ee} = 0.413 \pm 0.015$. For the $J/\psi + X$ channel, the constant-field scan efficiency is $\varepsilon_{\rm cf}^X = 0.402 \pm 0.011$; differences in detection efficiency between the two scans are accounted for by the parameter $(\varepsilon_{\rm co}^X / \varepsilon_{\rm cf}^X)$. They are due to a different configuration of the tracking system, which does not affect the e^+e^- channel. The likelihood maximization was performed within the R package [10] and crosschecked with the MINUIT code [11]. The results of the fit are shown in Figure 1, Figure 2, and Table 3. [3]

The fitted value of η in Table 3 is consistent with the one determined from the synchrotron frequency (Section 3). The relative uncertainty in the phase-slip factor (6%) is equal to that from the E760 double scans [4].

Possible statistical and systematic sources of uncertainty in the width and area are considered. As discussed in Section 3, each beam spectrum is a luminosity-weighted sum of individual energy distributions within each run. Statistical fluctuations of the BPM readings produce random variations of the measured ΔL which systematically widen the beam spectrum, making the resonance width narrower. The BPM noise is evaluated from portions of runs with no energy drifts and its standard deviation is 0.02 mm for both stacks. Thanks to hardware and software improvements, this is much lower than the E760 value, 0.2 mm [4]. The effect on width and area due to BPM noise is larger for small beam widths and for runs with no energy drifts. In the worst case, it translates into a systematic uncertainty of < 8 keV in the width and < 2 meV in the area. We do not correct for this systematic, but uncertainties are assigned to the results of 4 keV and 1 meV, respectively.

[3] The $\psi(2S)$ mass from Ref. [9] is used for the absolute calibration of L_0. The value of M in Table 3 is not an independent measurement.

The systematic uncertainties in the luminosity (2.5%) and e^+e^- efficiency (3.6%) directly affect the area, but not the width. They are added to obtain an uncertainty of 6.1% or 35 meV.

The absolute energy calibration does not influence the resonance width and area. Instead, a systematic error in the ΔL determination has the following effects: it shifts all runs in stack 1; it shifts stack 29 with respect to stack 1. The systematic uncertainty of 0.05 mm discussed in Section 3 translates into < 1 keV for the width and < 1 meV for the area, and it is therefore neglected. No systematic uncertainties are therefore introduced by combining the two scans. The pivot run in the constant-field scan (Section 4) is taken near the central orbit and has a small ΔL, so that its energy relative to the constant-orbit scan can be calculated accurately from Eq. 5.

Our final results are the following:

$$\Gamma = 290 \pm 25(\text{sta}) \pm 4(\text{sys}) \text{ keV} \tag{9}$$

$$\Gamma_{e^+e^-}\Gamma_{\bar{p}p}/\Gamma = 579 \pm 38(\text{sta}) \pm 36(\text{sys}) \text{ meV}. \tag{10}$$

6 Discussion

A comparison between this width measurement and those of E760 [4] and BES [1,2] is shown in Figure 3. All three values are consistent. The E835 measurement is the most precise. Our measurement of $(\Gamma_{e^+e^-}\Gamma_{\bar{p}p}/\Gamma)$ is also compatible, but much more precise, than that reported by BABAR, $\Gamma_{e^+e^-}\Gamma_{\bar{p}p}/\Gamma = 0.70 \pm 0.17 \pm 0.03$ eV [3].

This new method of complementary scans can be applied to future experiments for the direct determination of narrow resonance widths in antiproton-proton annihilations (such as PANDA at the future FAIR facility in Darmstadt). If one performs a scan at constant orbit and a scan at constant magnetic field in conditions similar to those in the Antiproton Accumulator, the uncertainty is mainly statistical. Moreover, by appropriately choosing the relative luminosities and energies of the two scans, one can make the width almost uncorrelated with the phase-slip factor, as in the E835 case discussed in this paper.

7 Acknowledgements

We gratefully acknowledge the support of the Fermilab staff and technicians and especially the Antiproton Source Department of the Accelerator Division and the On-line Department of the Computing Division. We also wish to thank the INFN and University technicians and engineers from Ferrara, Genoa, Turin and Northwestern for their valuable work. This research was supported by the Italian *Istituto Nazionale di Fisica Nucleare* (INFN) and the US Department of Energy.

References

[1] BES Collaboration, J. Z. Bai et al., Phys. Lett. B **550** (2002) 24

[2] BES Collaboration, M. Ablikim et al., Phys. Rev. Lett. **97** (2006) 121801

[3] BABAR Collaboration, B. Aubert et al., Phys. Rev. D **73** (2006) 012005

[4] E760 Collaboration, T. A. Armstrong et al., Phys. Rev. D **47** (1993) 772. We note that an error in the E760 calculation of initial-state radiation resulted in an overestimate of the $\psi(2S)$ and J/ψ widths. The corrected E760 results are $\Gamma_{\mathrm{E760}} = 287 \pm 37 \pm 16$ keV for the $\psi(2S)$ and $\Gamma_{\mathrm{E760}} = 91 \pm 11 \pm 6$ keV for the J/ψ.

[5] D. P. McGinnis, G. Stancari, and S. J. Werkema, Nucl. Instrum. Methods A **506** (2003) 205

[6] E835 Collaboration, G. Garzoglio et al., Nucl. Instrum. Methods A **519** (2004) 558

[7] D. C. Kennedy, Phys. Rev. D **46** (1992) 461

[8] E835 Collaboration, M. Andreotti et al., Phys. Rev. D **71** (2005) 032006

[9] V. M. Aulchenko et al., Phys. Lett. B **573** (2003) 63

[10] R Development Core Team (2005). R: A language and environment for statistical computing. R Foundation for Statistical Computing, Vienna, Austria. ISBN 3-900051-07-0, <http://www.R-project.org>

[11] F. James, MINUIT: Function Minimization and Error Analysis, Version 94.1, CERN Program Library Long Writeup D506.

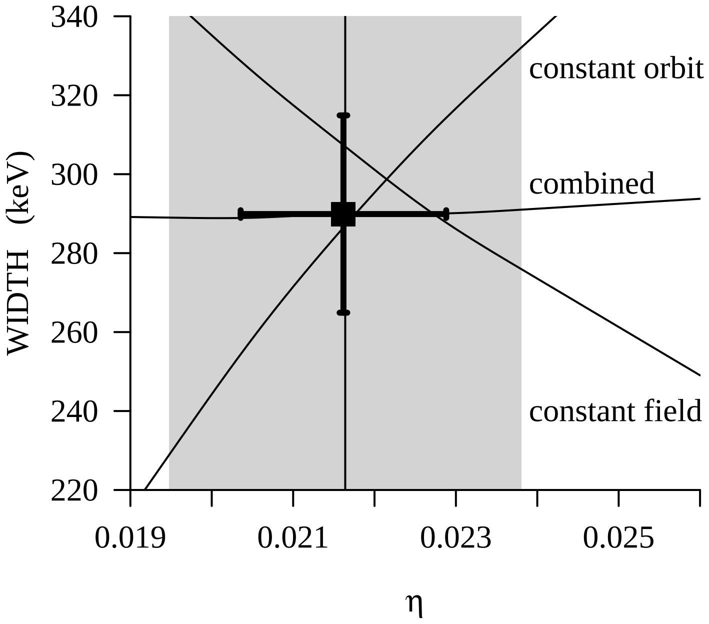

Fig. 1. Γ dependence on η for stacks 1 and 29, and from their combination, when the phase-slip factor is a fixed parameter. The result of the global fit with free η is represented by the cross. The value of the phase-slip factor from the synchrotron-frequency measurement (vertical line) and its uncertainty (gray band) are also shown.

Run	Energy	Luminosity	e^+e^- events	$J/\psi+X$ events
i	$w_i^{\rm rf}$ (MeV)	$\mathscr{L}_i$ (nb^{-1})	N_i^{ee}	N_i^X
5006	3687.585	15.20	0	1
5009	3687.632	37.20	1	3
5012	3687.373	44.40	0	8
5013	3687.343	42.20	0	5
5015	3687.121	37.20	0	5
5016	3687.080	45.10	2	11
5019	3686.760	80.80	5	18
5022	3686.471	41.58	5	45
5023	3686.453	37.15	4	32
5025	3686.012	98.56	67	280
5027	3685.678	15.88	12	26
5028	3685.667	45.37	19	76
5029	3685.848	43.44	20	85
5031	3685.643	80.99	18	67
5036	3685.338	21.22	1	9
5038	3685.334	61.43	4	13
		747.72	158	684

Table 1

Stack 1 data.

Run	Energy	Luminosity	e^+e^- events	$J/\psi+X$ events
i	$w_i^{\rm rf}$ (MeV)	$\mathscr{L}_i$ ($\rm nb^{-1}$)	N_i^{ee}	N_i^X
5818	3686.674	77.81	15	65
5819	3686.701	50.01	7	49
5821	3686.422	79.13	27	142
5822	3686.427	40.63	18	75
5824	3686.126	78.34	37	257
5825	3686.138	55.50	27	175
5827	3685.922	78.80	52	291
5828	3685.922	68.44	41	264
5830	3685.633	79.07	25	149
5831	3685.643	48.52	19	100
5833	3684.455	79.31	1	11
5834	3684.450	78.35	0	10
5837	3684.451	78.68	3	10
		892.59	272	1598

Table 2

Stack 29 data.

	Parameter	Value	Correlation matrix						
			2	3	4	5	6	7	8
1	M (MeV)	3686.111 ± 0.009	0.02	0.35	-0.07	-0.64	-0.23	0.10	-0.17
2	Γ (keV)	290 ± 25		0.35	-0.29	0.02	-0.07	0.05	-0.52
3	$\Gamma_{e^+e^-}\Gamma_{\bar{p}p}/\Gamma$ (meV)	579 ± 38			-0.44	-0.48	-0.28	-0.58	-0.27
4	$\sigma_{\rm bkg}(e^+e^-)$ (pb)	3 ± 6				0.09	0.07	0.28	0.17
5	η (10^{-4})	216 ± 13					0.54	-0.20	0.17
6	$\epsilon^X_{\rm co}/\epsilon^X_{\rm cf}$ (%)	73 ± 4						-0.29	0.02
7	$\frac{{\rm Area}(J/\psi+X)}{{\rm Area}(e^+e^-)}$	5.81 ± 0.35							-0.17
8	$\sigma_{\rm bkg}(J/\psi+X)$ (pb)	65 ± 19							
$[\log(\Lambda)]_{\rm max}$		-170.95							
Goodness-of-fit tests:									
	log-likelihood ratio	68.8 / 50 ($P = 4.0\%$)							
	χ^2 / d.o.f.	68.3 / 50 ($P = 4.3\%$)							

Table 3

Summary of the results of the maximum-likelihood fit.

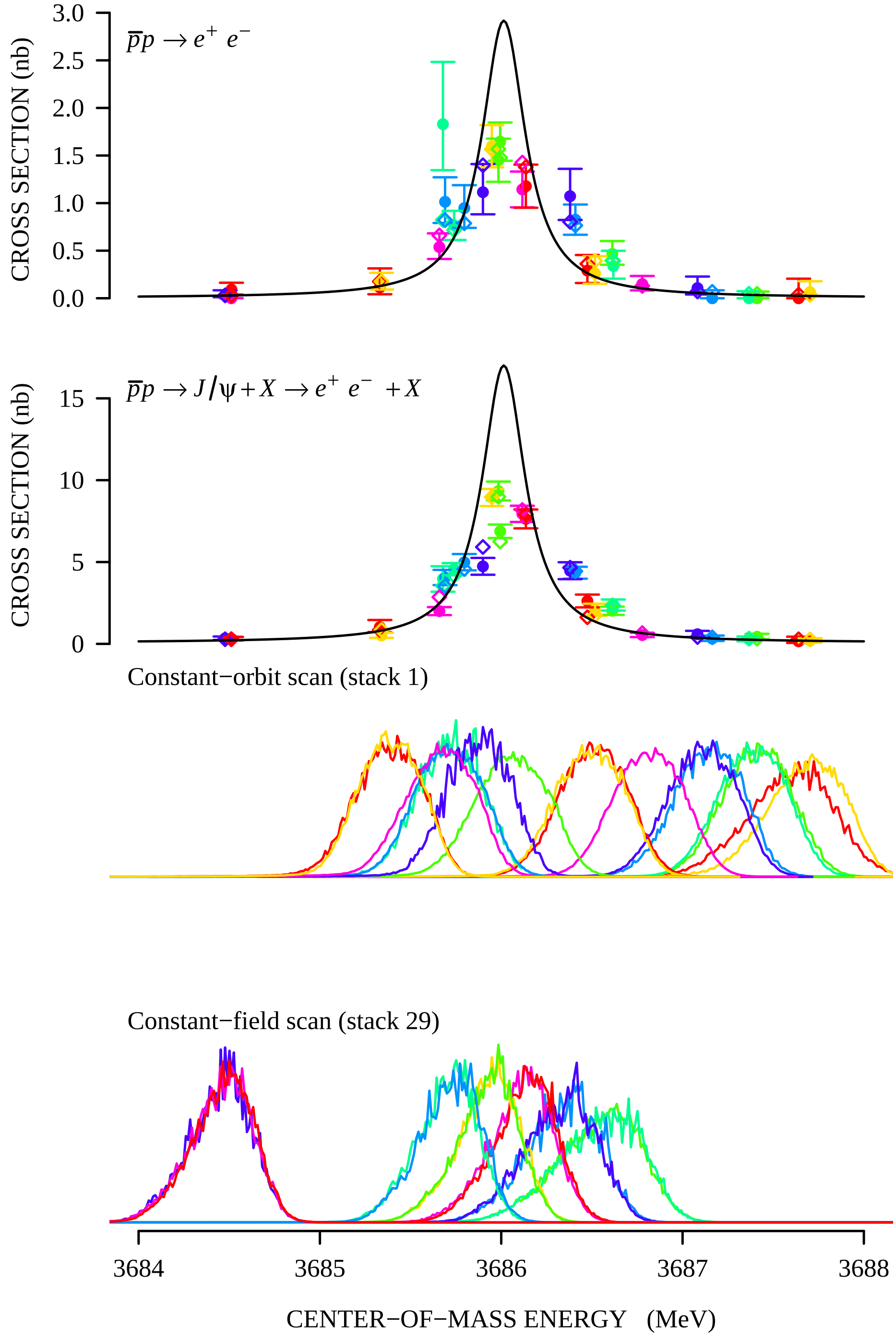

Fig. 2. $\psi(2S)$ resonance scans: the observed cross section for each channel (filled dots); the expected cross section from the fit (open diamonds); the 'bare' resonance curves σ_{BW} from the fit (solid lines). The two bottom plots show the normalized energy distributions B_i.

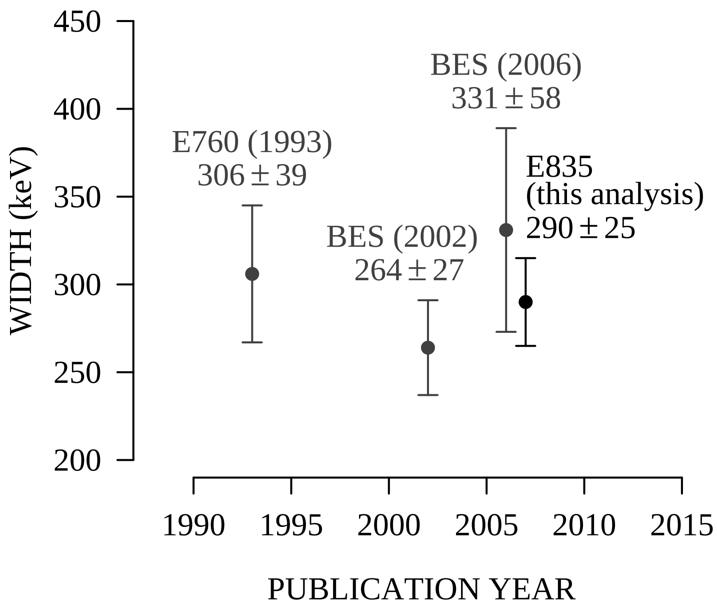

Fig. 3. Recent measurements of the $\psi(2S)$ width.